FULL PAPER

Dalton
www.rsc.org/dalton

A combined *para*hydrogen and theoretical study of H_2 activation by 16-electron d^8 ruthenium(0) complexes and their subsequent catalytic behaviour†

John P. Dunne,[a] Damir Blazina,[a] Stuart Aiken,[a] Hilary A. Carteret,[b] Simon B. Duckett,*[a] Jonathan. A. Jones,[c] Rinaldo Poli[d] and Adrian C. Whitwood[a]

[a] *Department of Chemistry, University of York, UK YO10 5DD*

[b] *LITQ, Departement d'Informatique et Recherche Operationelle, Universite de Montreal, Pavillon Andre-Aisenstadt, Montreal, Quebec H3C 3J7, Canada*

[c] *Oxford Centre for Quantum Computation, Clarendon Laboratory, Parks Road, Oxford, UK OX1 3PU*

[d] *Laboratoire de Chimie de Coordination, 205 Route de Narbonne, 31077 Toulouse Cedex, France*

Received 16th July 2004, Accepted 25th August 2004
First published as an Advance Article on the web 16th September 2004

The photochemical reaction of $Ru(CO)_3(L)_2$, where L = PPh_3, PMe_3, PCy_3 and P(*p*-tolyl)$_3$ with *para*hydrogen (*p*-H_2) has been studied by *in-situ* NMR spectroscopy and shown to result in two competing processes. The first of these involves loss of CO and results in the formation of the *cis*-*cis*-*trans*-L isomer of $Ru(CO)_2(L)_2(H)_2$, while in the second, a single photon induces loss of both CO and L and leads to the formation of *cis*-*cis*-*cis* $Ru(CO)_2(L)_2(H)_2$ and $Ru(CO)_2(L)(solvent)(H)_2$ where solvent = toluene, THF and pyridine (py). In the case of L = PPh_3, *cis*-*cis*-*trans*-L $Ru(CO)_2(L)_2(H)_2$ is shown to be an effective hydrogenation catalyst with rate limiting phosphine dissociation proceeding at a rate of 2.2 s^{-1} in pyridine at 355 K. Theoretical calculations and experimental observations show that H_2 addition to the $Ru(CO)_2(L)_2$ proceeds to form *cis*-*cis*-*trans*-L $Ru(CO)_2(L)_2(H)_2$ as the major product *via* addition over the π-accepting OC–Ru–CO axis.

Introduction

The examination of the oxidative addition of H_2 to d^8 square-planar transition metal complexes has been significant in enabling the understanding of how transition metal catalysts operate. For example, the accepted mechanism of H_2 addition to the square-planar $Ir(CO)Cl(PPh_3)_2$ is concerted and occurs across the Cl–Ir–CO axis.[1] Recent work in our group has shown that a minor product is also formed by H_2 addition over the P–Ir–P axis (Scheme 1).[2,3]

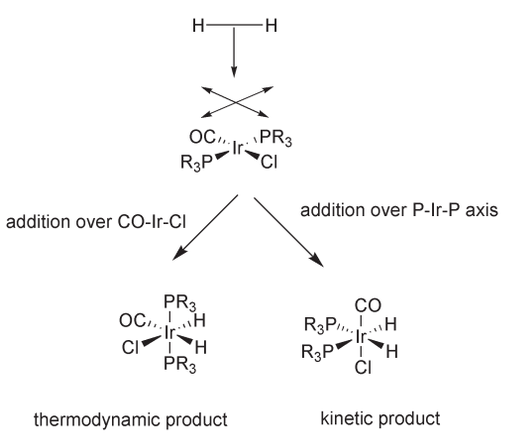

Scheme 1 Addition of H_2 to $IrCl(CO)(L)_2$ species.

We therefore set out to examine H_2 addition to the iso-electronic ruthenium species $Ru(CO)_2(L)_2$, where L = PPh_3, PMe_3, PCy_3 and P(*p*-tolyl)$_3$, and L_2 = dppe ($Ph_2PCH_2CH_2PPh_2$), which are formed by photolysis of $Ru(CO)_3(L)_2$ complexes. Ruthenium complexes of this type have attracted attention because of their ability to catalyse organic transformations.[4–10]

In 1965, Wilkinson and co-workers showed that $Ru(CO)_3(PPh_3)_2$ can catalyse the hydroformylation of alkenes to aldehydes,[4,5] and that this complex was converted to $Ru(CO)_2(PPh_3)_2(H)_2$, with *cis* carbonyls and hydrides, and mutually *trans* phosphine ligands (*cct*-L), before hydroformylation commenced.[6] Gordon and Eisenberg reported that this reaction can be initiated and accelerated photochemically.[7] Related ruthenium complexes such as $Ru(CO)(PPh_3)_3(H)_2$ have found use in catalytic C–C bond-forming reactions involving ketones and suitable alkenes.[8,9] Other ruthenium complexes have also been described that are successful in asymmetric hydrogenation.[10]

It is well known that a step in many catalytic transformations involves the binding of the transforming substrate to the catalyst. Hence, it is important to understand the selectivity shown by the addition of H_2 to potential catalysts, such as the ruthenium complexes that feature here. Recently, Caulton and co-workers isolated the 16-electron ruthenium(0) complex $Ru(CO)_2(PMe^tBu_2)_2$, which has a trigonal-bipyramidal structure with a vacant equatorial site.[11] This suggests that H_2 addition could take place either parallel or orthogonal to the OC–Ru–CO axis. Previous NMR studies on $Ru(CO)_2(L)_2(H)_2$ (L = PMe_3, PMe_2Ph, and $AsMe_2Ph$) have revealed that these compounds can exist in three geometries, *cis*, *cis*, *cis* (*ccc*), *cct*-L and *cct*-CO, with equilibrium ratios that are highly dependent on the electronic properties of L (see Scheme 2).[12–14] If these reactions involve the same $Ru(CO)_2(L)_2$ intermediate as characterised with L = PMe^tBu_2, then H_2 addition across both the ligand–metal axes could account for two of these products. When L = PMe_3, the *ccc* form proved to be visible only when *para*hydrogen (*p*-H_2)[13,14] was used to amplify its spectral features and hence studying this problem poses many challenges. In contrast, when L = $AsMe_2Ph$, the *ccc*- and *cct*-L forms were found to be present in similar quantities and a *cct*-CO isomer was detectable. At elevated temperatures, the $AsMe_2Ph$ complexes proved to be in equilibrium, while for the other systems dynamic behaviour was observed. Fluxional behaviour within $Ru(CO)_2(L)_2(H)_2$ could therefore also account

† Electronic supplementary information (ESI) available: NMR characterisation, catalytic studies, and *XYZ* coordinates determined for optimised structures. See http://www.rsc.org/suppdata/dt/b4/b410912k/

DOI: 10.1039/b410912k

for the observed product distribution. In the case of L_2 = dppe, hydride site interchange within the *ccc* form has been observed and shown to be accompanied by synchronised CO and phosphorus centre interchange. This process was suggested to involve the formation of a trigonal-bipyramidal transition state that contained an η^2-H_2 ligand with little H–H bonding character. Subsequent theoretical studies on the related $Ru(CO)_2(PH_2CH_2CH_2PH_2)(H)_2$ supported this view.[15] The potential fluxionality of these ruthenium dihydride species therefore complicates the original aim of exploring the addition of H_2 to $Ru(CO)_2(L)_2$.[13]

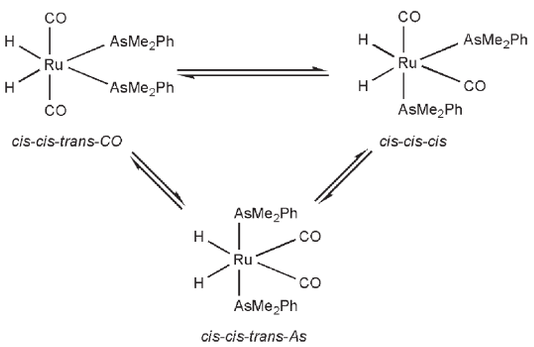

Scheme 2 Observed isomers of $Ru(AsMe_2Ph)_2(CO)_2(H)_2$.

There have been a number of reports on the use of UV photolysis of an NMR sample within the NMR probe to study *in-situ* reactions.[16–20] Here we have employed NMR spectroscopy in conjunction with *in-situ* photolysis and *p*-H_2 to study H_2 addition to a series of ruthenium complexes. Utilisation of the *p*-H_2 effect was necessary to allow low concentration photoproducts to be detected *via* the observation of enhanced NMR signals for nuclei that originate in the *p*-H_2 molecule. Recent photochemical studies in our group on $Ru(CO)_3$(dppe) have demonstrated that the hydride ligands of the product $Ru(CO)_2$(dppe)$(H)_2$ are enhanced by a factor of 28400.[21] That study indicated the feasibility of using *p*-H_2 to initialise an NMR quantum computer, and the molecules described in the current paper were initially prepared to test their suitability in such an application.

The *p*-H_2 effect has been called PHIP (*para*hydrogen induced polarisation)[22] and PASADENA (*para*hydrogen and synthesis allow dramatically enhanced nuclear alignment)[23] and has been extensively reviewed.[24–27] A notable achievement in this area that is relevant to this study is the demonstration by Aime *et al.* that $Os_3(\mu\text{-}H)_2(CO)_{10}$, a species with magnetically equivalent hydrides, can be enhanced,[28] and that the enhanced hydride signal arises *via* the involvement of an intermediate with inequivalent hydrides. Similar studies involving $Ru_3(CO)_{11}$(NCMe) yielded an enhanced emission signal for molecular hydrogen that indicated a reversible interaction of *p*-H_2 with the Ru_3 cluster containing inequivalent hydrides.[29] More recently, PHIP has been employed in the sensitisation of a hydroformylation product containing a single *p*-H_2 atom[30] and the transfer of polarisation *via* a ^{13}C nucleus to deuterium after the hydrogenation of a perdeuterated substrate.[31] It has also been successfully exploited in the study of catalytic transformations by mono-,[32,33] di-[34] and tri-nuclear[35] species.

This paper illustrates: (i) investigations into the mechanism of H_2 addition to 16-electron d^8 ruthenium(0) complexes of the type $Ru(CO)_2(L)_2$; (ii) the linking of experimental observations and high-level DFT calculations and (iii) the catalytic properties of $Ru(CO)_3(L)_2$ systems towards hydrogenation and hydroformylation.

Results and discussion

Photochemical reactions of $Ru(CO)_3(PPh_3)_2$

When a toluene-d_8 solution of $Ru(CO)_3(PPh_3)_2$, **1-PPh$_3$**, was irradiated with a 325-nm He/Cd CW laser at 255 K inside the NMR spectrometer, no reaction was observed according to ^{31}P NMR spectroscopy. However, when the photolysis was repeated on a fresh sample in the presence of 3 atm of *p*-H_2, the initial 32-scan ^1H NMR spectrum revealed the selective formation of the *cis-cis-trans*-L isomer of the known complex $Ru(CO)_2(PPh_3)_2(H)_2$, *cct*-**2-PPh$_3$**.[36] This was evident from the hydride signal that was seen for the two chemically equivalent hydride ligands of *cct*-**2-PPh$_3$** at δ −6.35 which showed an unexpected *p*-H_2 enhancement (Fig. 1). Since *p*-H_2 corresponds to H_2 in the antisymmetric nuclear spin state (αβ-βα), any reaction that leads to a product in which this spin encoding is retained will yield NMR signals that are derived from a non-Boltzmann spin population. In chemical reactions that produce a new molecule where the two hydrogen atoms become distinct (I and S), the atoms become separately addressable and under these conditions are described in the product operator formalism as providing I_zS_z magnetisation. This state leads to observable I_zS_x and I_xS_z terms which correspond to anti-phase signals, one for the I spin and one for the S spin, which are separated by J_{IS} (with hydrogen, J_{HH}). However, in the case of *cct*-**2-PPh$_3$** a more complicated situation results since the two hydrides should form part of an A_2 spin system; this will be commented on later in the text.

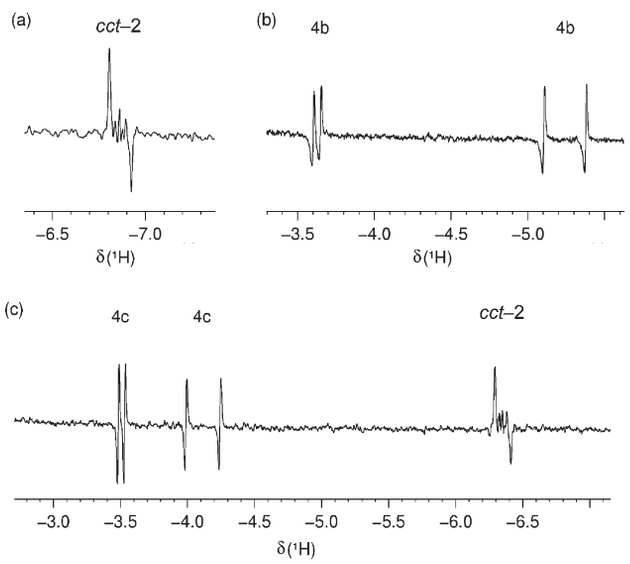

Fig. 1 Selected regions of NMR spectra obtained at 255 K during the reaction between $Ru(CO)_3(PPh_3)_2$ and *p*-H_2 with concurrent laser irradiation: (a) 32-transient ^1H spectrum of $Ru(CO)_2(PPh_3)_2(H)_2$, *cct*-**2**, in toluene-d_8; (b) ^1H spectrum illustrating the hydride resonances of $Ru(CO)_2(PPh_3)$(THF-d_8)$(H)_2$ **4b**; (c) ^1H spectrum in pyridine-d_5 showing $Ru(CO)_2(PPh_3)$(py-d_5)$(H)_2$ **4c**.

When a further 128 transients were recorded with concurrent photolysis, the new $^1H\{^{31}P\}$ NMR spectrum contained additional enhanced hydride resonances for the known *ccc* isomer of $Ru(CO)_2(PPh_3)_2(H)_2$, *ccc*-**2-PPh$_3$**, and weaker signals derived from the two equivalent hydride ligands of the *fac* isomer of the known complex $Ru(CO)_3(PPh_3)(H)_2$ and the two inequivalent hydrides of the corresponding *mer* isomer.[36] Appropriate NMR data for these complexes are provided in Table 1 and their structures are indicated in Fig. 2.

The formation of a further photoproduct became evident upon longer photolysis in spectra recorded with a large number of transients, where the greater signal intensities revealed two further hydride signals at δ −2.95 and −4.91, with 5% of the intensity of the signal for *cct*-**2-PPh$_3$**. These signals were assigned to **4a-PPh$_3$** and appeared as doublets of antiphase doublets, due to mutual J_{HH} couplings of −5 Hz and single ^{31}P couplings of 21 and 114 Hz, respectively. On stopping the laser irradiation, the hydride signals for all the products except *cct*-**2-PPh$_3$** decayed in intensity until after 1 min they were no longer observable. At this point the hydride signal for *cct*-**2-PPh$_3$**

Table 1 NMR data for complexes **2**–**4** and **6**, in toluene-d_8 at 273 K unless otherwise specified; see Fig. 2 for compound structures

Compound	$\delta(^1H)$	$\delta(^{31}P\{^1H\})$	$\delta(^{13}C\{^1H\})$[a]	$\delta(^{15}N\{^1H\})$[b]
cct-**2-PPh$_3$**	−6.35, 2nd order J_{HP} = 24 Hz, J_{HC} = 27 Hz (*cis* + *trans*)	56.5, s	202.0, t, J_{CP} = 9 Hz	
ccc-**2-PPh$_3$**	−6.27, dd, J_{HP} = 26 Hz (*cis*-P_A), 17 Hz (*cis*-P_B), J_{HH} = −6 Hz −7.28, dd, J_{HP} = 73 Hz (*trans*-P_A), 31 Hz (*cis*-P_B), J_{HH} = −6 Hz	50.2, d, J_{PP} = 28 Hz (P_A) 41.6, d, J_{PP} = 28 Hz (P_B)		
mer-**3-PPh$_3$**	−6.67, dd, J_{HP} = 15 Hz (*cis*), J_{HH} = −6 Hz −7.32, dd, J_{HP} = 61 Hz (*trans*), J_{HH} = −6 Hz	27.4, s		
fac-**3-PPh$_3$**	−6.65, 2nd order J_{HP} = 27 Hz, J_{HC} = 27 Hz (*cis* + *trans*), J_{HC} = 10 Hz (*cis*)	55.1, s	196.6, d, J_{PC} = 14 Hz (*cis*) 198.0, d, J_{PC} = 81 Hz (*trans*)	
4a-PPh$_3$	−2.95, dd, J_{HP} = 21 Hz (*cis*), J_{HH} = −5 Hz −4.91, dd, J_{HP} = 114 Hz (*trans*), J_{HH} = −5 Hz			
4b-PPh$_3$ (THF-d_8)	−3.66, dd, J_{HP} = 18 Hz (*cis*), J_{HH} = −6 Hz −5.26, dd, J_{HP} = 117 Hz (*trans*), J_{HH} = −6 Hz	41.9, s		
4c-PPh$_3$(OC-6–13) (py-d_5)	−3.52, dd, J_{HP} = 20 Hz (*cis*), J_{HH} = −7 Hz[c] −4.14, dd, J_{HP} = 101 Hz (*trans*), J_{HH} = −7 Hz[c]	45.6, s		248, d, J_{NP} = 16 Hz
4c′-PPh$_3$(OC-6–31) (py-d_5)	−4.44, dd, J_{HP} = 29 Hz (*cis*), J_{HH} = −7 Hz[c] −13.73, dd, J_{HP} = 26 Hz (*cis*), J_{HN} = 13 Hz (*trans*), J_{HH} = −7 Hz	27.0, s		
cct-**2-P(*p*-tolyl)$_3$**	−6.04, 2nd order, J_{HP} = 23 Hz	55.4, s		
mer-**3-P(*p*-tolyl)$_3$**	−6.50, dd, J_{HP} = 16 Hz (*cis*), J_{HH} = −5 Hz −7.28, dd, J_{HP} = 62 Hz (*trans*), J_{HH} = −5 Hz	36.2, s		
4a-P(*p*-tolyl)$_3$	−3.33, dd, J_{HP} = 19 Hz (*cis*), J_{HH} = −4 Hz −4.20, dd, J_{HP} = 102 Hz (*trans*), J_{HH} = −4 Hz			
4c-P(*p*-tolyl)$_3$	−3.50, dd, J_{HP} = 20 Hz (*cis*), J_{HH} = −4 Hz −4.49, dd, J_{HP} = 100 Hz (*trans*), J_{HH} = −4 Hz	42.5, s	203.6, *trans* to H 190.5, *cis* to H	
cct-**2-PMe$_3$**	−7.30, 2nd order, J_{HP} = 25 Hz	−0.5, s	202.4, t, J_{CP} = 9 Hz	
ccc-**2-PMe$_3$**	−7.37, ddd, J_{HH} = −5 Hz[d] −7.76, ddd, J_{HP} = 71 Hz (*trans*-P_A), 33 Hz (*cis*-P_B), J_{HH} = −5 Hz	−13.7, d, J_{PP} = 28 Hz (P_A) −4.3, d, J_{PP} = 28 Hz (P_B)		
4c-PMe$_3$(OC-6–13) (py-d_5)	−4.04, dd, J_{HP} = 23 Hz (*cis*), J_{HH} = −5 Hz[c] −4.25, dd, J_{HP} = 102 Hz (*trans*), J_{HH} = −5 Hz[c]	−11.8, s		
4c′-PMe$_3$(OC-6–31) (py-d_5, 315 K)	−4.55, dd, J_{HP} = 32 Hz (*cis*), J_{HH} = −7 Hz[c] −14.20, dd, J_{HP} = 27 Hz (*cis*), J_{HN} = 13 Hz (*trans*), J_{HH} = −7 Hz	7.0, s		
cct-**2-PCy$_3$**	−8.25, 2nd order, J_{HP} = 26 Hz	69.4, s	205.0, t, J_{CP} = 7 Hz	
mer-**3-PCy$_3$**	−7.33, dd, J_{HP} = 56 Hz (*trans*), J_{HH} = −7 Hz −7.49, dd, J_{HP} = 17 Hz, (*cis*), J_{HH} = −7 Hz	43.4, s	207.0, d, J_{CP} = 3 Hz	
4c-PCy$_3$ (OC-6–13) (py-d_5)	−3.79, dd, J_{HP} = 19 Hz (*cis*), J_{HH} = −4 Hz −4.73, dd, J_{HP} = 97 Hz (*trans*), J_{HH} = −4 Hz			
4c′-PCy$_3$ (OC-6–31) (py-d_5)	−5.23, dd, J_{HP} = 29 Hz (*cis*), J_{HH} = −7 Hz −16.89, dd, J_{HP} = 25 Hz (*cis*), J_{HH} = −7 Hz			
6, Ru(CO)(py)$_2$(H_2)	−2.00, d, J_{HH} = −8 Hz −11.26, d, J_{HH} = −8 Hz			

[a] ^{13}CO labelled sample (*ca.* 100% enriched). [b] ^{15}N labelled sample (*ca.* 100% enriched). [c] $^2J_{HN}$ hidden within the line width of the hydride resonance (indicative of a *cis* H–Ru–N arrangement). [d] Masked by overlap with *cct* isomer.

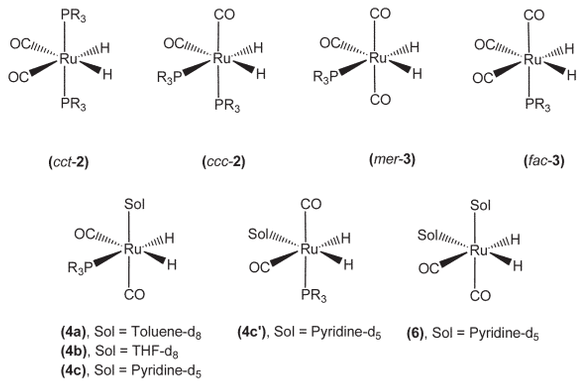

Fig. 2 Proposed structures for compounds **2**–**4** and **6** identified in this study, where R = Ph, Me, Cy or *p*-tolyl.

had a normal signal profile, which confirmed its hydride ligands do not exchange with free H_2 at this temperature. This information indicates that the hydride signals for *ccc*-**2-PPh$_3$**, *fac*-**3-PPh$_3$** and **4a-PPh$_3$** are only enhanced at 255 K because they are formed photochemically, and that they either convert to *cct*-**2-PPh$_3$** or are present in such low amounts as to be undetectable under normal conditions.

The identity of the previously unknown species **4a-PPh$_3$** was deduced by changing the solvent. When the same experiment was repeated in THF-d_8 at 255 K, a pair of analogous hydride signals were observed at δ −3.66 and −5.26 due to **4b-PPh$_3$** (Fig. 1). It should be noted that no enhanced hydride resonances corresponding to *ccc*-**2-PPh$_3$** were observed in spectra recorded in THF-d_8, although on longer photolysis hydride signals for *mer*- and *fac*-**3-PPh$_3$** were again detected. On moving to pyridine-d_5, a series of similar observations were made, with the related complex **4c-PPh$_3$** now exhibiting enhanced hydride resonances at δ −3.52 and −4.14 (Fig. 1). However, in pyridine-d_5, the hydride signals for *cct*-**2-PPh$_3$** and **4c-PPh$_3$** were equally intense at the onset of irradiation. Once again, the signals for *ccc*-**2-PPh$_3$** could not be observed. It should be noted that enhanced hydride signals for *cct*-**2-PPh$_3$** were immediately apparent in all these experiments.

These observations indicate that products of the type **4-PPh$_3$** correspond to the highly reactive solvent complex $Ru(CO)_2(PPh_3)$(solvent)$(H)_2$. The NMR signatures of these complexes require structures where phosphine and CO ligands are *trans* to the two hydrides. For **4b-PPh$_3$** and **4c-PPh$_3$** solvent coordination *via* a heteroatom lone pair is expected while in **4a-PPh$_3$** the toluene ligand is predicted to coordinate in an η^2-fashion.[16] Unfortunately, this reaction could not be examined in a non-coordinating solvent such as cyclohexane or methylcyclohexane due to the insolubility of **1-PPh$_3$** in these solvents. Under such conditions, the formation of the unsaturated 16-electron complex $Ru(CO)_2(PPh_3)(H)_2$ complex with a square-based pyramidal geometry and inequivalent equatorial hydride ligands would have been expected.[37] Since this complex would contain a hydride ligand that is *trans* to a vacant site and hence yield a hydride signal at very high field (δ −20 to −40),[38] any suggestion that **4a-PPh$_3$** contains a vacant coordination site can be discounted.

The effect of the solvent on this reaction is clearly substantial, since although *cct*-**2-PPh$_3$**, *mer* and *fac*-**3-PPh$_3$** and **4-PPh$_3$** were seen in THF and pyridine, signals for *ccc*-**2-PPh$_3$** were absent. In order to probe the effect of the coordinating strength of the solvent more directly, we examined a toluene-d_8 solution of **1-PPh$_3$** containing a 20-fold excess of PPh_3 and *p*-H_2 at 273 K. Signals for *mer* and *fac*-**3-PPh$_3$** and *ccc*-**2-PPh$_3$** were observed but with dramatically reduced signal intensities relative to the situation without phosphine, while signals for **4a-PPh$_3$** were absent. This study was then repeated in toluene-d_8 using 20 μL of pyridine instead of PPh_3. Under these conditions the formation of the toluene solvent complex **4a-PPh$_3$** was again suppressed, with *ccc*-**2-PPh$_3$**, *mer*- and *fac*-**3-PPh$_3$** and the pyridine complex **4c-PPh$_3$** now being observed. These data suggest that any **4a-PPh$_3$** that is formed under these conditions reacts with pyridine to yield **4c-PPh$_3$**, or with phosphine to re-form *cct*-**2-PPh$_3$** more rapidly than the NMR detection time scale. The reduction in the observed signal strengths of the hydride resonances for *ccc*-**2-PPh$_3$** also suggests that one route to its formation involves the displacement of toluene in **4a-PPh$_3$** by CO. We note that no evidence for H–D exchange was observed in these experiments, so reversible hydride exchange with the solvent *via* C–H bond activation is not occurring.

Effect of phosphine on the product distribution

In order to probe the effect of the phosphine on this reaction, analogous complexes containing PMe_3, PCy_3, P(*p*-tolyl)$_3$ and the chelating diphosphine 1,2-bis(diphenylphosphino)ethane (dppe) were prepared and examined under identical conditions.

In the case of $Ru(CO)_3[P(p\text{-tolyl})_3]_2$ (*viz.* **1-P(*p*-tolyl)$_3$**), photolysis in toluene-d_8 at 255 K led to the initial observation of *cct*-$Ru(CO)_2[P(p\text{-tolyl})_3]_2(H)_2$, *cct*-**2-P(*p*-tolyl)$_3$**. The hydride signal for this species appears at δ −6.04 in the ^{1}H NMR spectrum, with a similar signal profile under these conditions to that described earlier for *cct*-**2-PPh$_3$**. On longer irradiation, hydride signals for *mer*-$Ru(CO)_3[P(p\text{-tolyl})_3](H)_2$, *mer*-**3-P(*p*-tolyl)$_3$**, and the toluene solvent complex **4a-P(*p*-tolyl)$_3$** were observed. No evidence was obtained in these spectra for the formation of the isomers *ccc*-**2-P(*p*-tolyl)$_3$** and *fac*-**3-P(*p*-tolyl)$_3$**. When the solvent was changed to pyridine-d_5, the major product proved to be *cct*-**2-P(*p*-tolyl)$_3$** and signals for the pyridine solvent complex **4c-P(*p*-tolyl)$_3$** were detected. Appropriate resonances for these species are listed in Table 1.

When a sample containing $Ru(CO)_3(PMe_3)_2$ (*viz.* **1-PMe$_3$**) was photolysed under *p*-H_2 in toluene-d_8 at 255 K only *cct*-**2-PMe$_3$** was observed.[13] Upon repeating this experiment at 295 K, hydride resonances for both the *cct* and *ccc* isomers of **2-PMe$_3$** were detected, although once irradiation was stopped the signals from *ccc*-**2-PMe$_3$** were no longer visible. The failure to observe the solvent complex **4c-PMe$_3$** or *mer*- and *fac*-**3-PMe$_3$** in this reaction suggests that the stronger donating ability of PMe_3 reduces the propensity for photochemically induced phosphine loss. However, when **1-PMe$_3$** was photolysed in pyridine-d_5 in the presence of three atm of *p*-H_2 at 255 K, very weak signals for a pair of enhanced hydride resonances at δ −4.04 and −4.25 due to **4c-PMe$_3$** were observed. The formation of *ccc*-**2-PMe$_3$** was again quenched.

In order to investigate the effect of introducing a more sterically demanding phosphine, the complex $Ru(CO)_3(PCy_3)_2$ was prepared. Crystals suitable for X-ray analysis were grown from a 1 : 1 mixture of THF–hexane at room temperature. This complex adopts a trigonal-bipyramid geometry (Fig. 3 and Tables 2 and 3) with equatorial CO groups and mutually *trans* axial tricyclohexylphosphine ligands. The cyclohexyl groups adopt a staggered orientation relative to the $Ru(CO)_3$

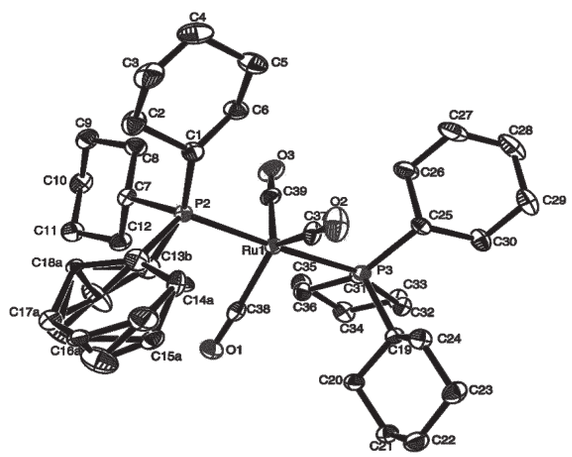

Fig. 3 Crystal structure of $Ru(CO)_3(PCy_3)_2$.

Table 2 Crystal data and structure refinement for $Ru(CO)_3(PCy_3)_2$ **1-PCy$_3$**

Empirical formula	$C_{39}H_{66}O_3P_2Ru$
Formula weight	745.93
Temperature/K	115(2)
Wavelength/Å	0.71073
Crystal system	Monoclinic
Space group	$P2_1/n$
Unit cell dimensions	
a/Å	15.587(2)
b/Å	12.4953(18)
c/Å	19.860(3)
β/°	95.843(4)
V/Å^3	3848.0(9)
Z	4
D_c/Mg m^{-3}	1.288
μ/mm^{-1}	0.525
F(000)	1592
Crystal size/mm	0.43 × 0.26 × 0.15
Theta range for data collection/°	1.58 to 27.53
Index ranges, hkl	−20 to 20, −16 to 13, −18 to 25
Reflections collected	25489
Independent reflections (R_{int})	8828 (0.0470)
Completeness to theta	27.53° → 99.6%
Absorption correction	None
Refinement method	Full-matrix least-squares on F^2
Data/restraints/parameters	8828/0/450
Goodness-of-fit on F^2	0.964
Final R indices [$I > 2\sigma(I)$]	$R1$ = 0.0320, $wR2$ = 0.0668
R indices (all data)	$R1$ = 0.0533, $wR2$ = 0.0725
Largest diff. peak, hole/e Å^{-3}	0.541, −0.485

Table 3 Relevant bond lengths and angles for $Ru(CO)_3(PCy)_3$ **1-PCy$_3$**

C(37)–Ru(1)	1.910(2)	C(13B)–P(2)	1.874(5)
C(38)–Ru(1)	1.903(2)	C(19)–P(3)	1.852(2)
C(39)–Ru(1)	1.915(2)	C(25)–P(3)	1.8679(19)
P(2)–Ru(1)	2.3783(6)	C(31)–P(3)	1.8792(19)
P(3)–Ru(1)	2.3788(6)	C(37)–O(2)	1.162(2)
C(1)–P(2)	1.864(2)	C(38)–O(1)	1.161(2)
C(7)–P(2)	1.856(2)	C(39)–O(3)	1.154(2)
C(13A)–P(2)	1.885(5)		
O(2)–C(37)–Ru(1)	178.0(2)	C(38)–Ru(1)–C(37)	119.74(9)
O(1)–C(38)–Ru(1)	176.60(18)	C(38)–Ru(1)–C(39)	116.77(9)
O(3)–C(39)–Ru(1)	175.26(19)	C(37)–Ru(1)–C(39)	123.49(9)
P(2)–Ru(1)–P(3)	176.942(19)		

core. This structure is directly analogous to that reported for related ruthenium complexes such as $Ru(CO)_3(PPh_3)_2$[39] and $Ru(CO)_3(PMe_3)_2$.[40] The Ru–P distances were found to be identical at 2.378 Å while the Ru–CO bond lengths differ slightly (1.910(2), 1.903(2), 1.915(2) Å). Notably, the Ru–P bond length is longer than that reported for the related PMe_3 complex where it is 2.34 Å. The P_{ax}–Ru–P_{ax} angle in **1-PCy$_3$** is slightly bent at 176.942(19)° with the CO_{eq}–Ru–CO_{eq} angles being inequivalent at 116.77(9), 119.74(9) and 123.49(9)°; all the O–C–Ru angles are also slightly bent away from linearity (*e.g.* 176.60°). It should also be noted that one of the cyclohexyl rings of a phosphine ligand is disordered due to conformational effects.

Photolysis of **1-PCy$_3$** with *p*-H_2 in toluene-d_8 at 253 K exclusively yielded the *cct*-**2-PCy$_3$** isomer with no evidence for a solvent dihydride analogous to **4a** or for the *ccc* isomer being obtained. In addition, no evidence for the formation of the *ccc*-**2** isomer was found even when these experiments were repeated at 295 K. This selectivity can be attributed to the steric bulk of tricyclohexylphosphine, which should disfavour the required *cis* arrangement in *ccc*-**2-PCy$_3$**. When the photolysis was performed in pyridine-d_5, NMR signals for two isomers of $Ru(CO)_2(PCy_3)(py)(H)_2$ were evident (Table 1).

Utilisation of a bidentate phosphine

Photolysis of $Ru(CO)_3$(dppe) in the presence of H_2 exclusively yielded the *ccc* isomer of the dihydride $Ru(CO)_2$(dppe)$(H)_2$ **5** in toluene-d_8.[13] In this species, one hydride ligand is *trans* to a ^{31}P centre and the other *trans* to CO. However, when the photolysis is performed in pyridine-d_5 two new minor species can be observed (see Fig. 4). The first of these, **5a**, shows ^{1}H signals at δ −3.89 (J_{HH} = −5 Hz, J_{HP} = 21 Hz) and −4.36 (J_{HH} = −5 Hz, J_{HP} = 104 Hz), which are split by a single phosphorus nucleus. The ^{31}P centre giving rise to these couplings was located at δ 39.17 by HMQC spectroscopy. The presence of the solitary ^{1}H–^{31}P coupling indicates that **5a** corresponds to a species in which the dppe ligand is unchelated, *i.e.* $Ru(CO)_2(\eta^1$-dppe$)(py)(H)_2$. From the hydride chemical shifts, the pyridine moiety can be deduced to be *cis* to both hydrides, with one hydride *trans* to phosphine and the other *trans* to CO, as shown in Fig. 5. It should be noted that due to the unstable nature of this species and the need for *p*-H_2 amplification, the uncoordinated ^{31}P centre could not be detected at this point.

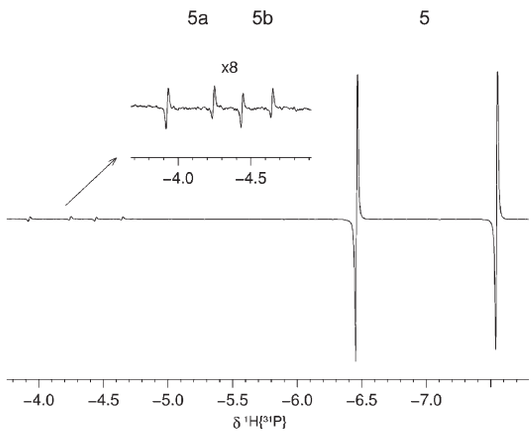

Fig. 4 ^{1}H{^{31}P} PHIP-enhanced spectrum at 275 K with concurrent photolysis, showing species **5**, **5a** and **5b**.

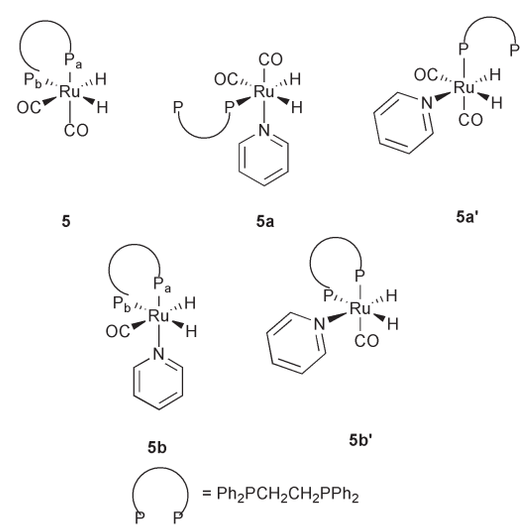

Fig. 5 Products formed from reactions of $Ru(CO)_3$(dppe) with 3 atm of *p*-H_2 in pyridine-d_5.

The second species, **5b**, exhibits ^{1}H hydride resonances at δ −4.46 and δ −4.65 (J_{HH} = −5 Hz), both of which couple to two ^{31}P nuclei. The second of these resonances exhibits a large ^{31}P coupling of 122 Hz to a ^{31}P nucleus resonating at δ 89.05 which is indicative of a *trans* arrangement between the associated ligands. A second coupling of 23 Hz was present due to a further ^{31}P centre that was detected at δ 65.41 in the corresponding ^{31}P NMR spectrum; the size of the J_{HP} is now indicative of a *cis* arrangement of the respective nuclei. The hydride resonance at δ −4.46, meanwhile, showed two *cis* couplings of 24 and 30 Hz to ^{31}P nuclei as detailed in Table 4.

On the basis of these data, **5b** can be concluded to be a second type of solvent complex, Ru(CO)(dppe)(py)$(H)_2$,

Table 4 NMR data for the products formed in the reaction of $Ru(CO)_3(dppe)$ with 3 atm of *p*-H_2 in pyridine-d_5 at 335 K

Compound	$\delta(^1H)$	$\delta(^{31}P\{^1H\})$
$Ru(H)_2(CO)_2(dppe)$ (**5**)	−6.46, ddd, J_{HP} = 22 Hz (*cis*-P_a), J_{HP} = 72 Hz (*trans*-P_b), J_{HH} = −5 Hz	65.2, P_b, d, J_{PP} = 13 Hz
	−7.55, ddd, J_{HP} = 19 Hz (*cis*-P_a), J_{HP} = 27 Hz (*cis*-P_b), J_{HH} = −5 Hz	71.7, P_a, d, J_{PP} = 13 Hz
$Ru(H)_2(CO)_2(\eta^1$-dppe)(py) OC-6–13 (**5a**)	−3.89, dd, J_{HP} = 21 Hz (*cis*), J_{HH} = −5 Hz	39.17, d, J_{PP} = 50 Hz
	−4.36, dd, J_{HP} = 104 Hz (*trans*), J_{HH} = −5 Hz	
$Ru(H)_2(CO)_2(\eta^1$-dppe)(py) OC-6–31 (**5a′**)	−4.77, dd, J_{HP} = 26 Hz (*cis*), J_{HH} = −7 Hz	49.5
	−13.97, dd, J_{HP} = 27 Hz (*cis*), J_{HH} = −7 Hz	
$Ru(H)_2(CO)$(dppe)(py) OC-6–13 (**5b**)	−4.46, ddd, J_{HP} = 24 Hz (*cis*-P_a), J_{HP} = 30 Hz (*cis*-P_b), J_{HH} = −5 Hz	65.41, P_a, d, J_{PP} = 16 Hz
	−4.65, ddd, J_{HP} = 122 Hz (*trans*-P_b), J_{HP} = 23 Hz (*cis*-P_a), J_{HH} = −5 Hz	89.05, P_b, d, J_{PP} = 16 Hz
$Ru(H)_2(CO)$(dppe)(py) OC-6–14 (**5b′**)	−4.61, unknown multiplicity	45.5, P_b
	−16.38, ddd, J_{HP} = 16 Hz (*cis*), J_{HP} = 29 Hz (*cis*) J_{HH} = −7 Hz	76.0, P_a

where the dppe ligand is coordinated in a bidentate fashion and the pyridine moiety is *cis* to both hydrides (Fig. 5). Comparable amounts of **5a** to **5b** are formed on the basis of the corresponding hydride signal intensities (5 : 4). However, if it is assumed that identical hydride enhancements are seen on a per mole basis for each of the three products, **5a** and **5b** are formed at 1% of the level of **5**.

Thermal reactions of $Ru(CO)_3(L)_2$ complexes

Previous reports indicate that heating a toluene-d_8 solution of **1-PPh$_3$** to 335 K in the presence of *p*-H_2 yields a mixture of *cct*-**2-PPh$_3$** (major product), *ccc*-**2-PPh$_3$**, *mer*-**3-PPh$_3$** and *fac*-**3-PPh$_3$**.[36] We have repeated this reaction in pyridine-d_5 and found the same core product distribution as seen in the photochemical studies described above, although two additional hydride containing products were evident. The first of these showed enhanced hydride resonances at δ −4.44 and −13.73. Both these resonances appeared as doublets of antiphase doublets due to *cis* ^1H–^{31}P couplings of 29 and 26 Hz, respectively; the ^{31}P nucleus was located at δ 27.0 by HMQC methodology. The chemical shifts of these resonances indicate that while the former is *trans* to CO, the latter is *trans* to pyridine. This identifies this species as further isomer of the pyridine solvent complex, **4c′** (see Fig. 2 for structure). The identity of **4c′** was confirmed by repeating the experiment with ^{15}N-labelled pyridine. Under these conditions, the resonance at δ −13.73 exhibited a 13 Hz *trans* coupling to ^{15}N but in the case of **4c′-PPh$_3$**, the low intensity of the hydride resonances precluded the determination of the bound pyridine's ^{15}N chemical shift. The coordinated pyridine ligand of **4c-PPh$_3$** was, however, located at δ 248 by HMQC methods.

The second new product detected in these spectra, **6**, yielded hydride resonances at δ −2.0 and −11.26. Both of these appeared as simple antiphase doublets (J_{HH} = −8 Hz), suggesting that **6** does not contain a phosphine ligand and that it therefore corresponds to the double substitution product *ccc*-$Ru(CO)_2(py)_2(H)_2$. It is worth noting that species of type **4c** and **4c′** are also observed under thermal conditions when 20 μL of pyridine is added to toluene-d_8 solution of **1-PPh$_3$** under H_2. In contrast, species **6** is only observed under these conditions in neat pyridine. This concentration dependence supports the assignment of **6** as the double substitution product. We further note that both **4c′** and **6** were absent from the photochemical studies and were only detectable under thermal conditions.

Another surprising feature of these *p*-H_2 based ^1H NMR spectra was noted when they were recorded at or above 335 K, in both pyridine-d_5 and toluene-d_8. Under these conditions, an enhanced peak was visible at δ +7.89. This corresponds to a signal for the *ortho*-phenyl protons of the PPh_3 ligands in *cct*-**2-PPh$_3$**. EXSY investigations and ^2H labelling experiments demonstrated that there was no exchange between hydride and *ortho*-phenyl proton sites in this species. However, high-resolution COSY spectra employing *p*-H_2 enabled the detection of a small (0.05 Hz) spin–spin coupling between the protons in these two locations.

We have previously commented in this paper that the appearance of the hydride resonance of *cct*-**2-PPh$_3$** at δ −6.35 was unusual because the antiphase components of the *p*-H_2 enhanced signal are separated by 2 × J_{HP} rather than the more usual J_{HH} value. Since the two hydride ligands of *cct*-**2-PPh$_3$** are in chemically identical environments, an A_2 spin system would be expected and no signal enhancement should be seen. The observation of an enhanced hydride resonance, however, implies that these two nuclei actually belong to a complex second-order spin system. Several examples of *p*-H_2 based signal enhancements under such circumstances have been reported.[28,41,42] The weak spin-spin coupling between the hydride ligands and the twelve *ortho*-phenyl protons of *cct*-**2-PPh$_3$** results in a complex spin system where the two chemically equivalent, but strongly coupled, phosphine ligands add to the complexity. This effect accounts for the hydride signal enhancement seen in complexes of the type *cct*-$Ru(CO)_2(L)_2(H)_2$. For analogous *cct*-**2** species containing different phosphines, the enhancement is suggested to arise *via* similar interactions between the hydrides and the corresponding protons on the phosphine ligands.

When a toluene-d_8 solution of the complex **1-PMe$_3$** was heated in the presence of *p*-H_2, no reaction was observed until 355 K; at this point hydride signals for both *cct*-**2-PMe$_3$** and *ccc*-**2-PMe$_3$** were observed. This corresponds to the point where Ru–CO bond breakage in **1-PMe$_3$** occurs. In contrast to the PPh_3 system, no monophosphine species such as $Ru(CO)_3(PMe_3)(H)_2$ were detected, which suggests that the Ru–PMe_3 bonds remain intact under these conditions. Furthermore, the addition of a small amount of PMe_3 to the system resulted in substantial hydride signal enhancements being observed for the known complex $Ru(H)_2(CO)(PMe_3)_3$.[43] However, when a sample of **1-PMe$_3$** was heated in the presence of *p*-H_2 in pyridine-d_5, the enhanced hydride resonances of *cct* and *ccc*-**2-PMe$_3$** were seen at 315 K. It can therefore be concluded that pyridine facilitates the CO substitution process. The product distribution in this reaction is significant and will be commented on later. However, it should be noted at this point that the largest set of hydride signals corresponded to a pair of doublets of antiphase doublets at δ −4.04 and −4.25 that arose from **4c-PMe$_3$**. This observation suggests that pyridine also facilitates the loss of CO and PMe_3 from **1-PMe$_3$**. Heating this sample further to 355 K in the presence of *p*-H_2 resulted in the observation of the second isomer of the solvent complex, **4c′-PMe$_3$**, as well as the double solvent substitution product **6**.

Upon heating a sample of **1-P(*p*-tolyl)$_3$** in pyridine-d_5 to 355 K under *p*-H_2, the complexes *cct*-**2-P(*p*-tolyl)$_3$**, *ccc*-**2-P(*p*-tolyl)$_3$**, *mer*-**3-P(*p*-tolyl)$_3$** were seen, as were weaker signals for the solvent complexes **4c-P(*p*-tolyl)$_3$**, **4c′-P(*p*-tolyl)$_3$** and **6**. In contrast, heating **1-PCy$_3$** under identical conditions yielded only *cct*-**2-PCy$_3$** and the solvent complexes **4c-PCy$_3$**, **4c′-PCy$_3$** and **6**. The failure to observe *mer*-**3** and *fac*-**3** with the strongly basic phosphines PMe_3 and PCy_3 will be commented on further in the section on catalytic behaviour.

On examining $Ru(CO)_3(dppe)$ under *p*-H_2 in pyridine-d_5 at 315 K in the absence of photolysis, enhanced hydride signals corresponding to species **5**, **5a** and **5b** were again detected. In contrast to photochemical investigations, where **5** was clearly

dominant, the ratio of **5**:**5a**:**5b** under thermal conditions was 1:1:1, assuming identical extents of enhancement on a per-mole basis. On increasing the temperature to 335 K, **5a** became the major species, exhibiting twice the signal intensities of the other two. This indicates that heating $Ru(CO)_3$(dppe) in pyridine facilitates the de-chelation of the dppe ligand. In addition, species **6** was observed, as were four new signals due to products present at approximately 3% of the level of **5a**. The first of these species yielded signals, at δ −4.77 and −13.97, which were shown to couple to each other in the corresponding COSY spectrum. Both these hydride signals appeared as doublets of antiphase doublets, which indicates that they originate in a species that contains an unchelated dppe ligand. The chemical shift of the latter hydride resonance suggests it arises from a hydride ligand that is *trans* to pyridine. This species is therefore assigned to **5a′**, an isomeric form of **5a** (see Table 4 and Fig. 5). The final two resonances, which also coupled to one another, appeared at δ −4.61 and −16.38. The multiplicity of the lower field resonance could not be determined because of signal overlap; however, the higher field hydride appeared as a doublet of doublets of antiphase doublets. This splitting pattern is indicative of two *cis* ^{31}P couplings and, given the chemical shift, arises from a hydride that is *trans* to pyridine. This species therefore corresponds to **5b′**, a further isomer of **5b** with the structure shown in Fig. 5. It should be noted that the low signal intensity for **5a′** and **5b′** precluded the determination of J_{PP} values from the associated HMQC spectra.

Theoretical examination of the 16-electron $Ru(CO)_2(L)_2$ intermediates

We have already commented on the experimental determination of the structure of $Ru(CO)_2(PMe^tBu_2)_2$ as a trigonal bipyramid with axial phosphines.[11] The X-ray structure of this species indicates that the associated vacant equatorial position is not stabilised by an agostic interaction with C–H bonds of the phosphine ligand. However, with less sterically demanding phosphines, other isomers of such 16-electron species might exist in solution. Three isomers **A**, **B** and **C** are possible as shown in Fig. 6. Upon H_2 addition to these 16-electron fragments, three isomers of $Ru(CO)_2(L)_2(H)_2$ can be formed, with (i) all *cis* ligand arrangements, (ii) *cis* hydrides and CO's and *trans* phosphines and (iii) *cis* hydrides and *cis* phosphines and *trans* CO's. In the case of $AsMe_2Ph$, as noted previously, all three of these geometries can be detected in solution.[13,42]

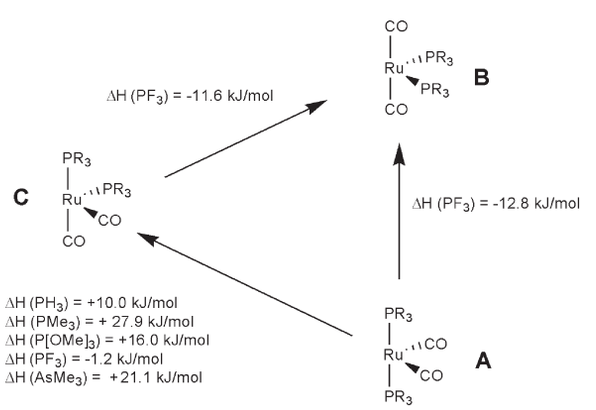

Fig. 6 Relative energies calculated for the 16-electron intermediates.

Theoretical work has previously been devoted to the analysis of RuL_4 species.[11,15,44–47] For the specific case of $Ru(CO)_2(L)_2$, MP2 calculations have been carried out on **A-PH$_3$** to confirm the preference for the experimentally observed nonplanar C_{2v} structure, whereas the isoelectronic $[Rh(CO)_2(PH_3)_2]^+$ species prefers a planar geometry.[11,46] Subsequent DFT studies at a theory level closely related to ours have calculated the structure of $Ru(CO)_2(H_2PCH_2CH_2PH_2)$, whose geometry is constrained as **C**, to model the experimentally observed compound with a $Bu^t_2PCH_2CH_2PBu^t_2$ ligand. For the simpler PH_3 system, isomer **C** was found to be 5.5 kJ mol^{-1} less stable than isomer **A**.[47] No information was reported on isomer **B**. In a separate study, we also carried out calculations on $Ru(CO)_2(H_2PCH_2CH_2PH_2)$ which focused on studying the size of the singlet–triplet energy gap in comparison with the analogous Fe system.[15] We have now carried out DFT calculations to examine the structural arrangements and the relative energies of the three possible isomers of $Ru(CO)_2(L)_2$ when L = PH_3, PMe_3, $P(OMe)_3$, $AsMe_3$ and PF_3. Since the chemistry involved here concerns only the singlet state, and since the triplet was shown to have a significantly higher energy for both the PH_3[47] and the $H_2PCH_2CH_2PH_2$[15] systems at ruthenium, we have confined our calculations to the singlet state.

The calculations reported here were carried out using the same level of theory previously employed for $Fe(CO)_2(PH_3)_2$,[48] where a benchmark investigation demonstrated that it gave the most reliable results for $Fe(CO)_4$.[49]

With PH_3 as the phosphine, the most stable isomer was found to correspond to **A-PH$_3$**, which is 10 kJ mol^{-1} lower in energy than **C-PH$_3$**. This result parallels that already reported by Eisenstein and coworkers.[47] The corresponding isomer with equatorial phosphines **B-PH$_3$** failed to optimise, converting instead to **A-PH$_3$**. Changing the phosphine to trimethylphosphine gave a similar result, with isomer **A-PMe$_3$** now being 27.9 kJ mol^{-1} more stable than **C-PMe$_3$**. The same relative energy profile is also found with trimethyl phosphite where **A-P(OMe)$_3$** is 16.0 kJ mol^{-1} lower in energy than **C-P(OMe)$_3$**. These data suggest that the introduction of an increased π-accepting ability in the phosphine lowers the energy difference between the two isomeric forms. To test this hypothesis the strongly π-acidic phosphine PF_3 was examined. In this case the lowest energy isomer proved to be **B-PF$_3$**, which was now 11.6 kJ mol^{-1} lower in energy than **C-PF$_3$**, which was in turn 1.2 kJ mol^{-1} lower in energy than **A-PF$_3$**. These data confirm that the strongest π-acceptor prefers to locate itself in an equatorial site as previously suggested.[11] In the case of L = $AsMe_3$, the relative energies of **A-AsMe$_3$** and **C-AsMe$_3$** differ by 21.1 kJ mol^{-1}, a difference which although lower than that found for PMe_3 is very similar to the $P(OMe)_3$ value. The similar relative proportions of the *ccc* and *cct*-L isomers of $Ru(CO)_2(AsMe_2Ph)_2(H)_2$ observed experimentally cannot therefore be attributed simply to the relative energies of these intermediates.

Relevant optimised distances and angles for these species are shown in Table 5. All optimised **A** isomers have very similar geometries, with the axial P–Ru–P angle being close to 170° and the equatorial OC–Ru–CO angle close to 135°. The axial Ru–P bonds were found to bend slightly towards the empty equatorial site. These parameters are in relatively good agreement with those experimentally determined for $Ru(CO)_2(PMe^tBu_2)_2$ where the corresponding angles are 166.5° and 133.3° respectively.[11] As shown previously,[47] the potential energy surface along the coordinate corresponding to the opening and closing of these angles is rather flat, and wide structural changes may be expected as a result of minor changes in the ligands. The Ru–L distances are, however, quite similar for PH_3 (2.304 Å) and PMe_3 (2.304 Å), whereas they significantly shorten on going to the stronger π-acids $P(OMe)_3$ (2.295 Å) and PF_3 (2.229 Å) but lengthen for $AsMe_3$. These distances do, however, compare well with the experimentally determined value of 2.357 Å for the PMe^tBu_2 complex.[11] The equatorial Ru–CO distances show a much smaller variation across the series.

The failure to detect a *cct*-CO H_2 addition isomer in all the phosphine systems examined here with *p*-H_2 suggests that the barrier to H_2 addition over the P–Ru–P axis of isomer **A** of $Ru(CO)_2(L)_2$ exceeds 20 kJ mol^{-1}. This value is deduced on the basis of the potential 15000-fold enhancement that could be observed in this reaction with *p*-H_2 at 253 K.

The optimised structures corresponding to isomer **C** show a greater variability of angular parameters. However, the overall

Table 5 Selected bond lengths (Å) and bond angles (°) for all calculated $Ru(CO)_2(L)_2$ fragments using B3PW91* level of theory

Compound	M–L_{ax}/Å	M–L_{eq}/Å	L_{ax}–X/Å	L_{eq}–X/Å	L_{ax}–M–L_{ax}/°	L_{eq}–M–L_{eq}/°
$Ru(CO)_2(PH_3)_2$ (**A-PH$_3$**)	2.304	1.902	1.154	1.434	171.2	138.7
$Ru(CO)_2(PH_3)_2$ (**C-PH$_3$**)	1.864 (C)	1.859 (C)	1.154 (CO)	1.556 (CO)	95.9	92.1
	2.330 (P)	2.358 (P)	1.425 (PH_3)	1.427 (PH_3)		
$Ru(CO)_2(PMe_3)_2$ (**A-PMe$_3$**)	2.304	1.875	1.850 (P)	1.159 (CO)	170.0	135.3
$Ru(CO)_2(PMe_3)_2$ (**C-PMe$_3$**)	2.370 (P)	2.364 (P)	1.841 (P)	1.841 (P)	151.5	151.5
	1.855 (CO)	1.855 (CO)	1.159 (CO)	1.160 (CO)		
$Ru(CO)_2(PPh_3)_2$ (**A-PPh$_3$**)	2.309	1.862	1.827	1.165	162.4	127.9
$Ru(CO)_2(PPh_3)_2$ (**C-PPh$_3$**)						
$Ru(CO)_2(PF_3)_2$ (**A-PF$_3$**)	2.2291	1.89864	1.594	1.1466	166.89	135.93
$Ru(CO)_2(PF_3)_2$ (**B-PF$_3$**)	1.938	2.178	1.140	1.602	167.22	123.5
$Ru(CO)_2(PF_3)_2$ (**C-PF$_3$**)	2.250 (P)	1.886 (P)	1.594 (P)	1.611 (P)	164.3	128.4
	1.918 (CO)	1.886 (CO)	1.141 (CO)	1.147 (CO)		
$Ru(CO)_2\{P(OMe)_3\}_2$ (**A-P(OMe)$_3$**)	2.295	1.876	1.622	1.160	169.3	133.5
$Ru(CO)_2\{P(OMe)_3\}_2$ (**C-P(OMe)$_3$**)	2.300 (P)	2.323 (P)	1.626 (P)	1.638 (P)	143.9	150.4
	1.871 (CO)	1.871 (CO)	1.155 (CO)	1.155 (CO)		
$Ru(CO)_2(AsMe_3)_2$ (**A-AsMe$_3$**)	2.433	1.869	1.973	1.1179	170.4	131.5
$Ru(CO)_2(AsMe_3)_2$ (**C-AsMe$_3$**)	2.486 (As)	2.486 (As)	1.991 (As)	1.978 (As)	151.1	151.1
	1.852 (CO)	1.852 (CO)	1.171 (CO)	1.172 (CO)		

[a] All species were optimised in C_1 symmetry.

difference between the axial and equatorial P–Ru–C bond angles is always smaller than that found in isomer **A** and in the case of PMe_3 they are the same. Eisenstein and coworkers have proposed that such a ligand arrangement features in the transition state for site exchange when L = PH_3; this was found to be only 1.3 kJ mol^{-1} higher in energy than isomer **C**. Thus, depending on the phosphine, this geometry may become a local energy minimum, which again highlights the flatness of the potential energy surface along this reaction coordinate. All the Ru–P distances were found to be longer in isomer **C** than in the corresponding isomer **A**. This is most likely a direct consequence of the *trans* influence of CO *vs*. phosphine but may reflect the steric cost of bringing the phosphine ligands closer together.

The geometry for isomer **B** yielded a stable minimum only for the PF_3 analogue. Here, the Ru–PF_3 distance is shorter than that in isomer **A**, a situation that is reversed when the Ru–CO distance is considered. This observation confirms the greater π-basicity of the metal with respect to the equatorial interactions, a phenomenon that has been previously highlighted.[44,46]

Relative ground-state energies of the *cct*-L and *ccc* isomers of $Ru(CO)_2(L)_2(H)_2$, L = PH_3, PMe_3 and $AsMe_3$

In the case of reactions with monodentate-phosphine containing precursors $Ru(CO)_3(L)_2$, the first species observed upon photolysis proved to be *cct*-L $Ru(CO)_2(L)_2(H)_2$, *cct*-**2-L**. This product geometry can be formed by loss of an equatorial CO ligand from **1**, followed by H_2 addition over the OC–Ru–CO axis of intermediate **A** (Scheme 3). However, accounting for the formation of *ccc*-**2**, as well as species **3** and **4**, *at low temperature* is more complex. For instance, *ccc*-**2** could be formed by re-arrangement of intermediate **A** to **C** followed by H_2 addition, or from *cct*-**2** by ligand re-arrangement (Scheme 3). The relative energies of the dihydrides therefore also need to be assessed.

The calculated structures for the dihydride species $Ru(CO)_2(L)_2(H)_2$ (where L = PH_3, PMe_3 and $AsMe_3$) optimise with distorted octahedral geometries (Table 6). Their basic structure is, however, similar to that reported for the related Fe(II) complex, *tcc*-$Fe(CO)_2[P(OPh)_3]_2H_2$.[50,51] In the case of L = PH_3, calculations show that the *ccc* isomer of $Ru(CO)_2(PH_3)_2(H)_2$ is favoured over the *cct*-PH_3 isomer by 12.7 kJ mol^{-1}. In contrast, when the L = PMe_3 the *cct*-L isomer is favoured by 19.6 kJ mol^{-1}. For $AsMe_3$, the calculated relative energies of the isomers at 295 K are much closer with the *cct* isomer being 9.42 kJ mol^{-1} more stable than the *ccc* isomer, and 17.71 kJ mol^{-1} more stable than the *ccc*-CO isomer. These relative energies are consistent with experimentally observed isomer populations of both the $Ru(CO)_2(PMe_3)_2(H)_2$ and $Ru(CO)_2(AsMe_2Ph)_2(H)_2$ systems under thermal conditions and confirm that it is the relative energies of the 18-electron products, not the 16-electron intermediate $Ru(CO)_2(L)_2$ that is important in controlling the product distribution. This deduction is consistent with the fact that at elevated temperatures, the corresponding $AsMe_2Ph$ complexes proved to be in equilibrium.[13,42]

Mechanistic considerations at low temperature

In the low-temperature photochemical studies described here, the quenching of *ccc*-**2-PPh$_3$** and *ccc*-**2-PMe$_3$** in coordinating solvents such as pyridine suggests that isomer interchange *via* the *cct*-L form at low temperatures is not responsible for the observation of the *ccc* isomer.

In order to investigate this process further, authentic samples of *cct*-**2-PPh$_3$** and *cct*-**2-PCy$_3$** were prepared and irradiated. Under these conditions, concurrent 325-nm irradiation did not lead to the observation of any new species in the corresponding ^{1}H NMR spectra. The photochemical formation of $Ru(CO)_2L(H)_2$ from *cct*-**2** does not therefore account for the observation of *ccc*-**2** or **4**.

These observations suggest that the starting $Ru(CO)_3(L)_2$ complexes must be able to undergo photochemical ejection of both CO and PPh_3 to form the 14-electron intermediate $Ru(CO)_2(L)$. This intermediate subsequently yields the solvent dihydride complexes **4** and both *ccc*-**2** and **3**, a deduction consistent with the fact that pyridine quenches the formation of *ccc*-**2** and **3**. Further support for this proposal comes from the observation that under photochemical conditions, the addition of CO to a sample of **1** under *p*-H_2 suppresses the formation of all the dihydride species, while the addition of free phosphine allows the formation of *cct*-**2** but suppresses the formation of the solvent complexes, as well as yielding the known trisphosphine dihydride species $Ru(CO)(PPh_3)_3(H)_2$.[43]

The formation of the 14-electron intermediate $Ru(CO)_2(L)$ could occur in a one- or two-photon process. The use of a series of neutral density filters (25, 50, 75%) enabled us to show the ratio of *cct*-**2-PPh$_3$** to **4c-PPh$_3$** was independent of the photon flux and hence deduce that both compounds are formed in a one-photon process.[52] The existence of such processes has been invoked previously in the case of related iron analogues.[53,54]

In this manuscript we have not described the photochemical reactions of $Ru(AsMe_2Ph)_2(CO)_3$ or $Ru(AsPh_3)_2(CO)_3$ with *p*-H_2 because the corresponding dihydride products only contain one easily accessible NMR handle, and hence their unambiguous characterisation is almost impossible. We note, however, that when toluene-d_8 solutions of $Ru(AsMe_2Ph)_2(CO)_3$ is irradiated at 255 K, signals for the corresponding *ccc* isomers

Table 6 Selected calculated bond lengths (Å) and bond angles (°) for $Ru(CO)_2(L)_2H_2$ species using B3PW91* level of theory

Compound	$Ru–L_{ax}$/Å	$Ru–L_{eq}$/Å	$L_{ax}–M–L_{ax}$/°	$L_{eq}–M–L_{eq}$/°	H–M–H/°
$Ru(CO)_2(PH_3)_2(H)_2$ ***cct*-PH$_3$**	2.296 (P)	1.922 (CO) 1.659 (H)	156.7	100.2	82.0
$Ru(CO)_2(PH_3)_2(H)_2$ ***ccc*-PH$_3$**	2.329 (P) 1.882 (CO)	2.358 (P) 1.923 (CO)	158.2	100.7	82.7
$Ru(CO)_2(PMe_3)_2(H)_2$ ***cct*-PMe$_3$**	2.324 (P)	1.908 (CO) 1.665 (H)	157.7	99.6	82.7
$Ru(CO)_2(PMe_3)_2(H)_2$ ***ccc*-PMe$_3$**	2.353 (P) 1.879 (CO)	2.376 (P) 1.907 (CO)	158.1	97.2	82.9
$Ru(CO)_2(PMe_3)_2(H)_2$ ***cct*-CO**	1.906 (CO)	2.384 (P) 1.635 (H)	157.6	101.1	84.8
$Ru(CO)_2(AsMe_3)_2(H)_2$ ***ccc*-AsMe$_3$**	2.452 (As) 1.868 (CO)	2.477 (As) 1.910 (CO)	157.7	98.5	82.9
$Ru(CO)_2(AsMe_3)_2(H)_2$ ***cct*-CO**	1.907 (CO)	2.488 (As) 1.636 (H)	158.2	101.3	84.4
$Ru(CO)_2(AsMe_3)_2(H)_2$ ***cct*-AsMe$_3$**	2.428 (As)	1.915 (As) 1.678 (H)	157.4	99.6	81.9

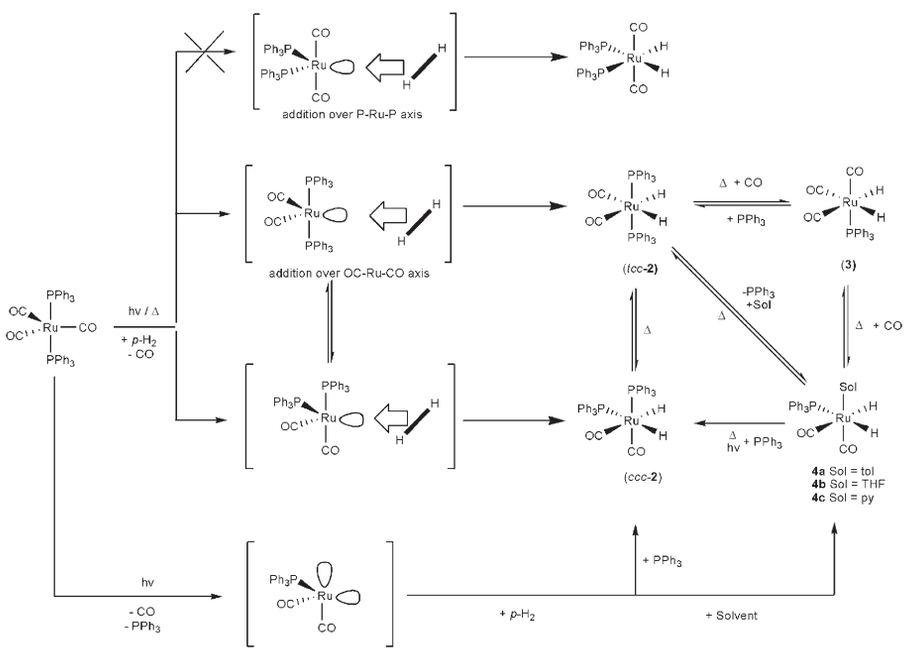

Scheme 3 Summary of mode of addition of H_2 to $Ru(CO)_2(PPh_3)_2$ fragments and subsequent reactions.

of the dihydrides are visible at δ −6.70 and −8.44 and the *tcc* isomer at δ −7.29. Upon changing the solvent to pyridine-d_5, the size of the signals due to the *ccc* isomers is substantially reduced, although on running these reactions at 295 K they again become strongly enhanced. These additional data fully support the previous deductions (Scheme 3). However, these are not the only signals that are seen in these spectra, and the situation with $AsPh_3$ is even more complex. These reactions are currently being explored in more detail.

Catalytic hydrogenation studies

A sample of **1-PPh$_3$** was then examined by NMR spectroscopy in pyridine-d_5 in the presence of *p*-H_2 and a 100-fold excess of diphenylacetylene (PhC≡CPh). When a sample was introduced into the NMR spectrometer at 335 K in the absence of photolysis, the hydride-containing species *cct*-**2-PPh$_3$** and **4c-PPh$_3$** were immediately observed in the corresponding ^{1}H NMR spectra. As the sample temperature increases to the set point, the signals for **4c-PPh$_3$** vanish and enhanced resonances due to *cis*-stilbene become evident, indicative of a thermally initiated hydrogenation reaction. It should be noted that when the experiment was repeated with concurrent UV irradiation, the intensity of both the hydride resonance of **2-PPh$_3$** and the enhanced *cis*-stilbene peak increased, which suggests that photochemical promotion of this reaction, although not required, is possible.[7] At 355 K, hydrogenation could be monitored directly and the rate quantified by EXSY methods. This was achieved *via* the monitoring of the transfer of magnetisation from the hydride resonance of *cct*-**2-PPh$_3$** into the hydrogenation product and free hydrogen (Fig. 7) as a function of reaction time. Analysis of these spectra was achieved by simulation.[55–58] The rate of H_2 transfer from **2-PPh$_3$** into *cis*-stilbene proved to be 2.2 s^{-1} while the rate of H_2 elimination was 3.1 s^{-1}. The observed rate constants obtained for these two processes proved to be independent of the alkyne excess relative to **1-PPh$_3$**. In comparison, the related trinuclear species $Ru_3(H)(\mu\text{-}H)(CO)_9(PPh_3)_2$ catalyses hydrogenation under much milder conditions (an apparent rate of 0.31 s^{-1} was observed at 300 K)[57,58] and at 355 K, hydrogenation by the cluster is fast on the NMR time scale, indicating (qualitatively) that the cluster is a better catalyst.

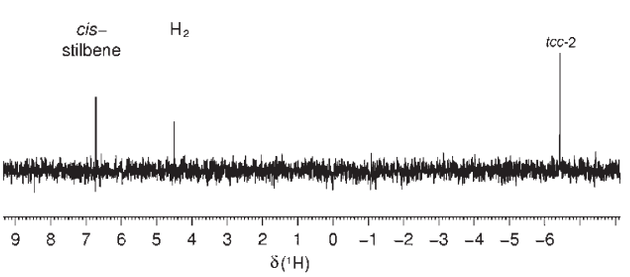

Fig. 7 EXSY spectrum depicting magnetisation transfer from *cct*-**2-PPh$_3$** to *cis*-stilbene and free H_2.

When toluene-d_8 was used as the solvent, no transfer of magnetisation from *cct*-**2-PPh$_3$** to *cis*-stilbene was observed at 355 K, but a *p*-H_2 enhanced signal for the hydrogenation product *cis*-stilbene was evident. It can therefore be concluded that catalytic hydrogenation does occur in toluene, but the associated rate is too slow to allow direct magnetisation transfer to be observed.

Since *cct*-**2-PPh$_3$** is coordinatively saturated, ligand loss must take place to facilitate catalysis. While the addition of 1 atm of CO to the system decreased the intensities of the hydride resonance for *cct*-**2-PPh$_3$** and the *cis*-stilbene peak, the measured rate of hydrogen transfer from **2-PPh$_3$** to *cis*-stilbene was unchanged. In contrast, the addition of a 50-fold excess of PPh_3 to the system essentially quenches the hydrogenation process. It can therefore be concluded that the first step in catalytic hydrogenation by **2-PPh$_3$** involves phosphine loss and the formation of the 16-electron intermediate $Ru(CO)_2(PPh_3)(H)_2$. Although the observation of the solvent complex **4c-PPh$_3$** is suppressed by the addition of PhC≡CPh, $Ru(CO)_2(PPh_3)$-(PhC≡CPh)$(H)_2$ is not detected at 355 K. This species has however been detected when $Ru_3(CO)_{10}(PPh_3)_2$ was examined with *p*-H_2 and PhC≡CPh in C_6D_6 at 300 K.[57,58] A complete catalytic cycle can therefore be assembled for this reaction, as shown in Scheme 4. In order to account for the dramatic solvent participation in the hydrogenation rate, we suggest that solvent participation assists in Ru–PPh_3 bond breakage.

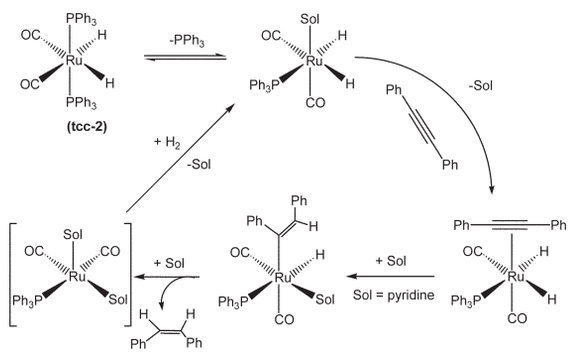

Scheme 4 Proposed catalytic cycle for hydrogenation of diphenylacetylene by *cct*-**2-PPh$_3$**.

The rate of hydrogenation by *cct*-**2-PPh$_3$** proved to be independent of the dihydrogen concentration. This indicates that dihydrogen transfer to the organic substrate and subsequent product elimination must occur before another H_2 molecule binds to the active species. This contrasts with the situation observed for $Ru_3(H)(\mu\text{-}H)(CO)_9(PPh_3)_2$, where the rate of hydrogenation was found to depend on the H_2 concentration.[57,58]

When samples of **1-PMe$_3$**, **1-P(*p*-tolyl)$_3$** and **1-PCy$_3$** were investigated as catalytic precursors, enhanced resonances for *cct*-**2** and *cis*-stilbene protons were again observed at 355 K, which are indicative of catalytic hydrogenation. However, the intensity of the *cis*-stilbene resonance was, in all three cases, lower than that seen with **1-PPh$_3$**, and no direct magnetisation transfer could be observed from *cct*-**2** species into *cis*-stilbene. This indicates that systems based on **1-PCy$_3$**, **1-P(*p*-tolyl)$_3$** and **1-PMe$_3$** are not as catalytically active as **1-PPh$_3$**. However, reductive elimination of H_2 from *cct*-**2-P(*p*-(tolyl)$_3$** and *cct*-**2-PMe$_3$** was still rapid enough to follow by EXSY methods. The associated rate constants at 355 K were 2.7 and 1.3 s^{-1}, respectively. Both these rates are slower than those found for *cct*-**2-PPh$_3$** under identical conditions and parallel the electron donating ability of the phosphine, which is expected to stabilise the dihydrides.

At long reaction times (16 h under catalytic conditions), stable resonances corresponding to *cct*-**2** and significant amounts of *cis*-stilbene were observed with all catalysts. In addition, slow isomerisation to *trans*-stilbene was evident in all cases, with approximately 5% of *cis*-stilbene being converted. This contrasts the situation with the trinuclear precursor $Ru_3(CO)_{10}(PPh_3)_2$, where only *cis*-stilbene was observed, even at prolonged reaction times.[57,58] Another interesting feature of this investigation was the observation of ^{31}P resonances corresponding to free phosphine ligands in all cases, which confirms that phosphine loss takes place during catalysis.

When $Ru(CO)_3$(dppe) was examined as the catalytic precursor, the resonances for **5**, **5a** and **5b** were again observed, as were polarised resonances for the hydrogenation product *cis*-stilbene. Interestingly, the resonances for **5b** were 5 times more intense than without substrate, indicating that this species now cycles hydrogen more rapidly and hence is an active hydrogenation catalyst. However, the rate of H_2 transfer to the hydrogenation product was again too slow to monitor directly by EXSY methods.

To examine this situation further, samples of **1-PPh$_3$**, **1-PCy$_3$**, **1-P(*p*-tolyl)$_3$**, **1-PMe$_3$** and $Ru(CO)_3$(dppe) were prepared with identical metal complex and substrate concentrations and were examined for catalytic hydrogenation under identical temperatures and H_2 pressures. Based on the build-up of *cis*-stilbene resonances over a period of 5 min, the catalytic activity order is PPh_3 > P(*p*-tolyl)$_3$ > PMe_3 > PCy_3 > dppe. The trend clearly shows that the electronic properties of the phosphine play a role in controlling catalysis with the more strongly donating phosphines being less suitable. Since catalysis is known to involve loss of a phosphine, it is clear that Ru–P bond breakage becomes more difficult as the basicity of the phosphine is increased, and hence catalysis is retarded. This is in agreement with the observation that **1-PCy$_3$** and **1-PMe$_3$**, with strongly basic phosphines, do not form the monophosphine species *mer*-**3** and *fac*-**3** under thermal conditions in toluene. In the case of dppe, the chelating nature of the phosphine makes phosphine loss less favourable and thus accounts for the low catalytic activity observed with this ligand.

When a sample of **1-PPh$_3$** was examined in the presence of diphenylacetylene, *p*-H_2 and CO, very slow build-up of a resonance at δ 9.84 due to an aldehydic proton was observed. This resonance is indicative of the presence of slow hydroformylation.

Conclusions

In this paper we have shown that photolysis of the compounds $Ru(CO)_3(L)_2$, where L = PPh_3, PMe_3, PCy_3 and P(*p*-tolyl)$_3$, in the presence of hydrogen, yields a product distribution that is dependent on the temperature and solvent. However, one species, *cis*-*cis*-*trans*-L $Ru(CO)_2(L)_2(H)_2$, is always produced, and is characterised by an unusual *para*hydrogen enhanced hydride resonance. This species proved unsuitable for quantum computation experiments, however, the study of this system has yielded valuable insights into the mechanisms of H_2 addition to d^8 Ru(0) complexes and their subsequent catalytic behaviour.

Photochemical addition of H_2 to $Ru(CO)_3(L)_2$ has been shown to proceed *via* initial loss of CO and the subsequent reaction of the $Ru(CO)_2(L)_2$ intermediate with hydrogen. Previous work indicates that the related species $Ru(CO)_2(PMe^tBu_2)_2$ adopts a trigonal-bipyramidal geometry with axial phosphines and a vacant equatorial site.[11] Hence, H_2 addition across the more π-accepting OC–Ru–CO axis readily accounts for the observation of *cct*-L $Ru(CO)_2(L)_2(H)_2$, while addition across the L–Ru–L axis is not observed, even with *p*-H_2 amplification. Literature studies on the laser-initiated reaction of $Ru(CO)_3$(dmpe) (dmpe = $Me_2PCH_2CH_2PMe_2$) with H_2 have described how CO dissociation leads to the rapid formation of $Ru(CO)_2$(dmpe)(solvent). On a longer timescale, reaction with H_2 leads to the generation of the stable complex $Ru(CO)_2(dmpe)(H)_2$.[59]

When the reaction is carried out in toluene, the photochemical formation of a second isomer of this species, *cis*-*cis*-*cis* $Ru(CO)_2(L)_2(H)_2$, does occur. Previous work has shown that this product is stable in its own right when L = $AsMe_2Ph$,[12,13]

but with phosphine ligands this minor isomer is only observed when $Ru(CO)_2(L)_2(H)_2$ is warmed with *p*-H_2, at which point the signal amplification of the associated hydride resonances allows its detection. The formation of *cis-cis-cis* $Ru(CO)_2(L)_2(H)_2$ cannot be achieved by the direct addition of H_2 to an $Ru(CO)_2(L)_2$ intermediate that is isostructural with $Ru(CO)_2(PMe^tBu_2)_2$. However, it may be possible to form this product by H_2 addition to a minor intermediate with *cis* phosphines. Theoretical calculations have revealed that when L = PMe_3, the isomer **A-PMe$_3$** with *trans* phosphines is 27.9 kJ mol^{-1} more stable than isomer **C-PMe$_3$** with *cis* phosphines (Fig. 6) necessary to form *ccc*-PMe_3 directly. If it is assumed that the *p*-H_2 based signal enhancement is at the theoretical maximum (a factor of 15000 is available with a simple 45° read pulse),[21] an isomer with an energy difference of 20 kJ mol^{-1} could be detected. The calculations therefore indicate that *cis-cis-cis* $Ru(CO)_2(PMe_3)_2(H)_2$ does not arise because of H_2 addition to **C-PMe$_3$**.

We have also described how the *in-situ* irradiation of $Ru(CO)_3(L)_2$ led to the detection of the solvent complexes $Ru(CO)_2(L)(sol)(H)_2$ (where sol is toluene, THF and pyridine). These species were shown to originate from the minor photoproduct $Ru(CO)_2(L)$, which is formed *via* a single photon pathway. This intermediate was shown to be responsible for the generation of *ccc*-$Ru(CO)_2(L)_2(H)_2$ as well as *fac* and *mer* isomers of $Ru(CO)_3(L)(H)_2$ at 253 K. This example serves to illustrate how the enhanced signal intensities provided by *para*-hydrogen in conjunction with high-level DFT calculations can be used to elucidate the mechanism of H_2 addition to a metal complex, and differentiate the mechanisms by which the various product isomers are formed.

Compounds of the type $Ru(CO)_3(L)_2$ also undergo thermal addition of H_2, and are active hydrogenation catalysts at elevated temperatures. The activity of the system is dependent on the phosphine, such that the most active system is produced when L = PPh_3. The catalytic activity also depends on the solvent, such that strongly coordinating solvents facilitate the catalytic process. In the most favourable case, the thermal generation of *cct*-PPh_3 $Ru(CO)_2(PPh_3)_2(H)_2$ in pyridine enabled direct magnetisation transfer into the hydrogenation product *cis*-stilbene to be observed. The mechanism of this transformation has been elucidated based on the direct detection of all the intermediates in the catalytic cycle and a rate of hydrogenation has been determined. At 355 K, catalytic hydrogenation proceeds *via* rate-limiting phosphine dissociation with a rate constant of 2.2 s^{-1}. The mechanistic information provided by this study represents the first step towards designing improved hydrogenation catalysts based on d^8 Ru(0) systems.

Experimental

General conditions and reagents

All reactions and purifications were carried out under nitrogen using glove-box, high-vacuum or Schlenk-line techniques. All chemicals were purchased from commercial suppliers and used without further purification.

NMR experiments

All NMR solvents (Apollo Scientific) were dried using appropriate methods and degassed prior to use. The NMR measurements were made using NMR tubes fitted with J. Young Teflon valves and solvents were added by vacuum transfer on a high vacuum line. For the *para*hydrogen induced polarization (PHIP) experiments, hydrogen enriched in the *para* spin state was prepared by cooling H_2 to 20 K over a paramagnetic catalyst (activated charcoal) as described previously.[60]

All NMR studies were carried out with sample concentrations of approximately 1 mM and spectra were recorded on a Bruker DRX-400 spectrometer with ^{1}H at 400.13 MHz, ^{31}P at 161.9 MHz, ^{13}C at 100.0 MHz and ^{15}N at 40.5 MHz, respectively. ^{1}H NMR chemical shifts are reported in ppm relative to residual ^{1}H signals in the deuterated solvents (toluene-d_7, δ 2.13, THF-d_7, δ 1.73 and pyridine-d_4, δ 8.74), ^{31}P NMR in ppm downfield of an external 85% solution of phosphoric acid, ^{13}C NMR relative to toluene-d_8, δ 21.3 and pyridine-d_5, δ 150.35 and ^{15}N relative to an external sample of CH_3NO_2. Modified COSY, HMQC and EXSY pulse sequences were used as previously described.[61–63]

In the hydrogenation studies, 1D EXSY spectra were acquired immediately after exposing the sample to hydrogen and introducing it into the probe. The results were modelled allowing for hydride transfer into the hydrogenation product, as described previously.[55–58] The rate constants obtained in this way were multiplied by two to take into account the analysis method.[64]

Synthesis of $Ru(CO)_3(L)_2$

1-PPh$_3$, **1-PMe$_3$**, $Ru(CO)_3(dppe)$, $Ru(AsMe_2Ph)_2(CO)_3$ and $Ru(AsPh_3)_2(CO)_3$ were prepared by literature procedures[6,65–67] and purified by recrystallisation from a hot solution of 1 : 1 THF–hexane. The synthesis of $Ru(CO)_3(PCy_3)_2$, **1-PCy$_3$**, followed a literature procedure[66] with purification by recrystallisation from a hot solution of 1 : 1 THF–hexane. NMR (toluene-d_8, 295 K): δ_H 1.34 (m), 1.68 (m), 1.85 (m), 2.27 (m), 2.41 (m); δ_P 49.0, (s); δ_C 202.0 (t, J_{C-P} = 9 Hz, CO), 38.60 (t, J_{C-P} = 11 Hz, C_{ipso}), 30.7 (s, C_{ortho}), 28.2 (t, J_{C-P} = 5 Hz, C_{para}), 27.0 (s, C_{meta}). Crystals of **1-PCy$_3$** suitable for X-ray diffraction were grown at room temperature from a 1 : 1 THF–hexane mixture.

The complex $Ru(CO)_3[P(p\text{-tolyl})_3]_2$, **1-P(*p*-tolyl)$_3$** was prepared by a modified literature procedure.[68] 2.7 g (9 mmol) of P(*p*-tolyl)$_3$ was dissolved in 100 ml of degassed 2-methoxyethanol and heated to reflux. To this solution was added 0.39 g (1.5 mmol) of $RuCl_3{\cdot}3H_2O$ dissolved in 30 ml of degassed 2-methoxyethanol, followed rapidly by 40 ml of degassed aqueous formaldehyde (37% wt) and 0.6 g potassium hydroxide dissolved in 30 ml of 2-methoxyethanol. This yellow solution was then reflux under nitrogen for 4 h by which time the product $Ru(CO)_3[P(p\text{-tolyl})_3]_2$ precipitated as yellow microcrystals. The solution was allowed to cool and the product filtered off. The yellow solid was washed with 20 ml of cold ethanol, then 10 ml of ice-cold water followed by 10 ml of ethanol and 30 ml of hexane. $Ru(CO)_3[P(p\text{-tolyl})_3]_2$ was recrystallised from a boiling solution of THF–hexane (2 : 1) to yield 845 mg (75% yield) of a pale yellow solid.

Preparation of $Ru(CO)_2(L)_2(H)_2$

To prepare the dihydride complexes $Ru(CO)_2(L)_2(H)_2$, where L = PCy_3 or PPh_3, a 50 mg sample of the corresponding complex $Ru(CO)_3(L)_2$ was dissolved in a minimum amount of dry toluene and degassed by three freeze–pump–thaw cycles. The sample was then filled with 1 atm of H_2 and photolysed under UV light (Xe-arc lamp) for 2 h, during which period the solution was degassed and refilled with fresh H_2 every 30 min. A gradual colour change from yellow to colourless was observed. The solvent was then removed *in vacuo* to yield a white powder corresponding to $Ru(CO)_2(L)_2(H)_2$, which was characterised by NMR spectroscopy and used without further purification.

In-situ photolysis

This was achieved using a modified NMR probe that was equipped for *in-situ* photolysis, as described previously.[16] A Kimmon IK3202R-D 325-nm He–Cd 27 mW continuous wave (CW) laser was used as the radiation source.

Computational details

All calculations were performed using the Gaussian 03 program[69] together with the modified form of the B3PW91 functional in conjunction with a flexible polarisable basis sets.[70] Specifically,

the c_3 coefficient in Becke's original three-parameter fit to thermochemical data[71] was changed to 0.15, to give the B3PW91* functional. Atoms C, O, P and As were described by the triple-zeta basis sets of Schäfer *et al.*[72] augmented by one d polarisation function on C, O, P, As (α = 0.8, 1.2, 0.55 and 0.34, respectively). The Ru atom was described with the SDD basis set,[70] which uses the Stuttgart/Dresden ECP and double-zeta functions for all valence electrons, augmented with an f polarisation function (α = 1). All minima were fully optimised and characterised by computing vibrational frequencies at the same level of theory.

Crystallography

Experimental details are collected in Table 2 and reported in the CIF file.

CCDC reference number 244908.

See http://www.rsc.org/suppdata/dt/b4/b410912k/ for crystallographic data in CIF or other electronic format.

Acknowledgements

We are grateful to the EPSRC, and the European Union for funding under the HYDROCHEM network (contract HPRN-CT-2002-00176) and to CINES for a grant of free computational time. We are also grateful for discussions with Prof. R. N. Perutz, Dr R. J. Mawby, Dr J. N. Moore and Dr J. Lynam and experimental help from Dr P. Callaghan.

References

1 L. Vaska and J. DiLuzio, *J. Am. Chem. Soc.*, 1961, **83**, 2784.
2 S. K. Hasnip, S. B. Duckett, C. J. Sleigh, D. R. Taylor, G. K. Barlow and M. J. Taylor, *Chem. Commun.*, 1999, 1717.
3 S. K. Hasnip, S. A. Colebrooke, C. J. Sleigh, S. B. Duckett, D. R. Taylor, G. K. Barlow and M. J. Taylor, *J. Chem. Soc., Dalton Trans.*, 2002, 743.
4 D. Evans, J. A. Osborn, F. H. Jardine and G. Wilkinson, *Nature*, 1965, **208**, 1203.
5 D. Evans, J. A. Osborn and J. Wilkinson, *J. Chem. Soc. A*, 1968, 3133.
6 R. A. Sanchez-Delgado, J. S. Bradley and G. Wilkinson, *J. Chem. Soc., Dalton Trans*, 1976, 399.
7 E. M. Gordon and R. Eisenberg, *J. Organomet. Chem.*, 1986, **306**, C53.
8 S. Murai, F. Kakiuchi, S. Sekini, Y. Tanaka, A. Kamatani, M. Sonoda and N. Chatani, *Nature*, 1993, **366**, 529.
9 R. F. R. Jazzar, M. F. Mahon and M. K. Whittlesey, *Organometallics*, 2001, **20**, 3745.
10 R. Noyori and T. Ohkuma, *Angew. Chem., Int. Ed.*, 2000, **40**, 40.
11 M. Ogasawara, S. A. MacGregor, W. E. Streib, K. Polting, O. Eisenstein and K. G. Caulton, *J. Am. Chem. Soc.*, 1995, **117**, 8869.
12 J. M. Bray and R. J. Mawby, *J. Chem. Soc., Dalton Trans.*, 1987, 2989.
13 S. B. Duckett, R. J. Mawby and M. G. Partridge, *Chem. Commun.*, 1996, 383.
14 D. Schott, C. J. Sleigh, J. P. Lowe, S. B. Duckett and R. J. Mawby, *Inorg. Chem.*, 2002, **41**, 2960.
15 D. Schott, J. P. Dunne, S. B. Duckett, C. Godard, J. N. Harvey, R. J. Mawby, G. Muller, R. N. Perutz, R. Poli and M. K. Whittlesey, *Dalton Trans.*, 2004, 3218.
16 C. Godard, P. L. Callaghan, J. L. Cunningham, S. B. Duckett, J. A. B. Lohman and R. N. Perutz, *Chem. Commun.*, 2002, 2836.
17 S. Geftakis and G. E. Ball, *J. Am. Chem. Soc.*, 1999, **121**, 6336.
18 N. A. Knatochnil, J. A. Pachinson, P. J. Bedmaishi and P. J. Sadler, *Angew. Chem., Int. Ed.*, 1999, **38**, 1460.
19 C. E. Lyon, J. L. Lopez, B. M. Cho and P. J. Hore, *Mol. Phys.*, 2002, **100**, 1261.
20 T. Kühn and H. Schwalbe, *J. Am. Chem. Soc.*, 2002, **122**, 6169.
21 M. S. Anwar, D. Blazina, H. A. Carteret, S. B. Duckett, T. K. Halstead, J. A. Jones, C. M. Kozak and R. J. K. Taylor, *Phys. Rev. Lett.*, 2004, **93**, 40501.
22 C. R. Bowers and D. P. Weitekamp, *J. Am. Chem. Soc.*, 1987, **109**, 5541.
23 T. C. Eisenschmid, R. U. Kirss, P. A. Deutsch, S. I. Hommeltoft, R. Eisenberg, J. Bargon, R. G. Lawler and A. L. Balch, *J. Am. Chem. Soc.*, 1987, **109**, 8089.
24 R. Eisenberg, *Acc. Chem. Res.*, 1991, **24**, 100.
25 J. Natherer and J. Bargon, *Prog. Nucl. Magn. Reson, Spectrosc.*, 1997, **31**, 293.
26 S. B. Duckett and C. J. Sleigh, *Prog. Nucl. Magn. Res. Spectrosc.*, 1999, **34**, 71.
27 S. B. Duckett and D. Blazina, *Eur. J. Inorg. Chem.*, 2003, 2901.
28 S. Aime, R. Gobetto and D. Canet, *J. Am. Chem. Soc.*, 1998, **120**, 6770.
29 S. Aime, W. Dastru, R. Gobetto, A. Russo, A. Viale and D. Canet, *J. Phys. Chem. A.*, 1999, **103**, 9702.
30 A. B. Permin and R. Eisenberg, *J. Am. Chem. Soc.*, 2002, **124**, 12406.
31 S. Aime, R. Gobetto, F. Raineri and D. Canet, *J. Chem. Phys.*, 2003, **119**, 8890.
32 A. Koch and J. Bargon, *Magn. Reson. Chem.*, 2000, **38**, 216.
33 M. Stephan, O. Kohlman, H. G. Niessen, A. Eichhorn and J. Bargon, *Magn. Reson. Chem.*, 2002, **40**, 157.
34 S. A. Colebrooke, S. B. Duckett and J. A. B. Lohman, *Chem. Commun.*, 2000, 685.
35 R. Gobetto, L. Milone, F. Reineri, L. Salassa, A. Viale and E. Rosenberg, *Organometallics*, 2002, **21**, 1919.
36 C. J. Sleigh, S. B. Duckett, R. J. Mawby and J. P. Lowe, *Chem. Commun.*, 1999, 1223.
37 R. H. Heyn, S. A. Macgregor, T. T. Nadasdi, M. Ogasawara, O. Eisenstein and K. G. Caulton, *Inorg. Chem. Acta.*, 1997, **259**, 5.
38 A. C. Cooper, W. E. Streib, O. Eisenstein and K. G. Caulton, *J. Am. Chem. Soc.*, 1997, **119**, 9069.
39 F. Dahan, S. Sabo and B. Chaudret, *Acta. Crystallogr. Sect. C: Cryst. Struct. Commun.*, 1984, **40**, 786.
40 R. A. Jones, G. Wilkinson, A. M. R. Galas, M. B. Hursthouse and K. M. A. Malik, *J. Chem. Soc., Dalton Trans.*, 1980, 1771.
41 M. Haake, J. Barkemeyer and J. Bargon, *J. Phys. Chem.*, 1995, **99**, 17539.
42 S. B. Duckett, R. J. Mawby and M. G. Partridge, *Chem. Commun.*, 1996, 383.
43 C. J. Sleigh, DPhil thesis, University of York, 1999.
44 M. Elian and R. Hoffmann, *Inorg. Chem.*, 1975, **14**, 1058.
45 J. Li, G. Schreckenbach and T. Ziegler, *J. Am. Chem. Soc.*, 1995, **117**, 486.
46 M. Ogasawara, S. A. Macgregor, W. E. Streib, K. Folting, O. Eisenstein and K. G. Caulton, *J. Am. Chem. Soc.*, 1996, **118**, 10189.
47 T. Gottschalk Gaudig, J. C. Huffman, H. Gérard, O. Eisenstein and K. G. Caulton, *Inorg. Chem.*, 2000, **39**, 3957.
48 J. N. Harvey and R. Poli, *Dalton Trans.*, 2003, 4100.
49 J. Harvey and M. Aschi, *Faraday Discuss.*, 2003, **124**, 129.
50 V. Arion, J. J. Brunet and D. Neibecker, *Inorg. Chem.*, 2001, **40**, 2628.
51 Nan Nhat Ho, R. Bau and S. A. Mason, *J. Organomet. Chem.*, 2003, **676**, 85.
52 I. K. Lednev, T. Q. Ye, L. C. Abbott, R. E. Hester and J. N. Moore, *J. Phys. Chem. A*, 1998, **102**, 9161.
53 V. Balcher, F. W. Grevels, K. Kerpen, G. Olbrich and K. Schaffner, *Organometallics*, 2003, **22**, 1696.
54 M. K. Kuimova, W. Z. Alsindi, J. Dyer, D. C. Grills, O. S. Jina, P. Matousek, A. W. Parker, P. Portius, X. Z. Sun, M. Towrie, C. Wilson, J. Yang and M. W. George, *Dalton Trans.*, 2003, 3996.
55 W. D. Jones, G. P. Rosini and J. A. Maguire, *Organometallics*, 1999, **18**, 1754.
56 D. Blazina, S. B. Duckett, P. J. Dyson, B. F. G. Johnson, J. A. B. Lohman and C. J. Sleigh, *J. Am. Chem. Soc.*, 2001, **123**, 9760.
57 D. Blazina, S. B. Duckett, P. J. Dyson and J. A. B. Lohman, *Angew. Chem., Int. Ed.*, 2001, **40**, 3874.
58 D. Blazina, S. B. Duckett, P. J. Dyson and J. A. B. Lohman, *Chem. Eur. J.*, 2003, **9**, 1046.
59 M. K. Whittlesey, R. N. Perutz, I. P. Virrels and M. W. George, *Organometallics*, 1997, **16**, 268.
60 M. S. Anwar, D. Blazina, H. A. Carteret, S. B. Duckett, T. K. Halstead, J. A. Jones and R. J. K. Taylor, *Magn. Reson. Chem.*, submitted.
61 B. A. Messerle, C. J. Sleigh, M. G. Partridge and S. B. Duckett, *J. Chem. Soc., Dalton Trans.*, 1999, 1429.
62 S. A. Colebrooke, S. B. Duckett and J. A. B. Lohman, *Chem. Commun.*, 2000, 685.
63 P. Hubler and J. Bargon, *Angew. Chem., Int. Ed.*, 2000, **39**, 3701.
64 M. L. H. Green, L. L. Wong and A. Sella, *Organometallics*, 1992, **11**, 2660.
65 K. Stott, J. Stonehouse, J. Keeler, T. L. Hwang and A. J. Shaka, *J. Am. Chem. Soc.*, 1995, **117**, 4199.
66 L. Song and W. C. Trogler, *J. Am. Chem. Soc.*, 1992, **114**, 3355.
67 G. Bellachioma, G. Cardaci, A. Macchioni and A. Madami, *Inorg. Chem.*, 1993, **32**, 554.

68 N. Ahmed, S. D. Robinson and M. F. Uttley, *J. Chem. Soc., Dalton Trans.*, 1972, 843.
69 *Gaussian 03*, Revision B.05. M. J. Frisch, G. W. Trucks, H. B. Schlegel, G. E. Scuseria, M. A. Robb, J. R. Cheeseman, J. A. Montgomery, Jr., T. Vreven, K. N. Kudin, J. C. Burant, J. M. Millam, S. S. Iyengar, J. Tomasi, V. Barone, B. Mennucci, M. Cossi, G. Scalmani, N. Rega, G. A. Petersson, H. Nakatsuji, M. Hada, M. Ehara, K. Toyota, R. Fukuda, J. Hasegawa, M. Ishida, T. Nakajima, Y. Honda, O. Kitao, H. Nakai, M. Klene, X. Li, J. E. Knox, H. P. Hratchian, J. B. Cross, C. Adamo, J. Jaramillo, R. Gomperts, R. E. Stratmann, O. Yazyev, A. J. Austin, R. Cammi, C. Pomelli, J. W. Ochterski, P. Y. Ayala, K. Morokuma, G. A. Voth, P. Salvador, J. J. Dannenberg, V. G. Zakrzewski, S. Dapprich, A. D. Daniels, M. C. Strain, O. Farkas, D. K. Malick, A. D. Rabuck, K. Raghavachari, J. B. Foresman, J. V. Ortiz, Q. Cui, A. G. Baboul, S. Clifford, J. Cioslowski, B. B. Stefanov, G. Liu, A. Liashenko, P. Piskorz, I. Komaromi, R. L. Martin, D. J. Fox, T. Keith, M. A. Al-Laham, C. Y. Peng, A. Nanayakkara, M. Challacombe, P. M. W. Gill, B. Johnson, W. Chen, M. W. Wong, C. Gonzalez, and J. A. Pople, Gaussian, Inc., Pittsburgh, PA, 2003.
70 J. Harvey and M. Aschi, *Faraday Discuss.*, 2003, **124**, 129.
71 A. D. Becke, *J. Chem. Phys.*, 1993, **98**, 5648–5652.
72 A. Schaefer, H. Horn and R. Ahlrichs, *J. Chem. Phys.*, 1992, **97**, 2571–2577.